

High-Fidelity Single-Image Head Modeling with Industry-Grade Topology

YUNMU WANG*, ZOUBIN BI*, BOWEN CAI*, CHENCHU RONG, JINLONG WANG, JUNCHEN DENG, AOCHENG HUANG, JIDONG JIA, and HUAN FU, Alibaba Group, China

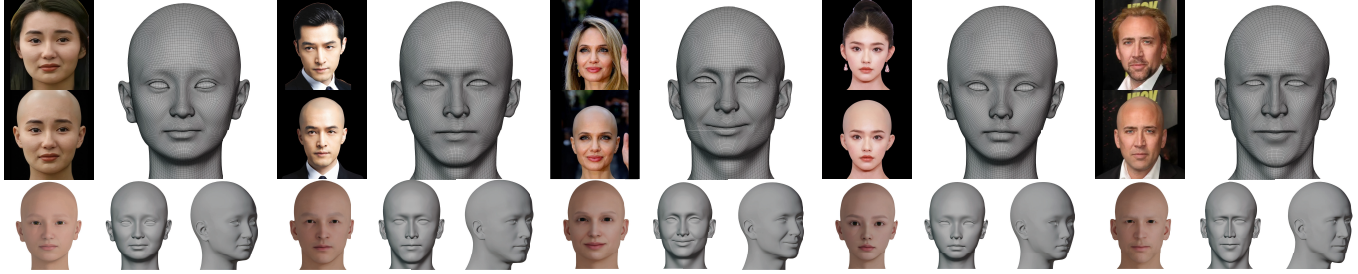


Fig. 1. **Single-image head modeling results of our method.** Our method generates high-fidelity, industry-grade head meshes with clean topology that can enter downstream binding and animation workflows. Frontalized and de-occluded inputs are shown for reference. Additional results are provided in the accompanying video and supplemental material. Please zoom in to inspect fine details.

We present a **single-image** head mesh reconstruction framework that addresses the longstanding challenge of simultaneously preserving **facial identity** and producing **industry-grade** topology. Our framework adopts a coarse-to-fine optimization pipeline that refines a rigged template across three stages—rig, joint, and vertex—achieving stable convergence and consistent topology. To mitigate the ill-posed nature of single-image 3D face reconstruction and ensure identity preservation, we employ a normal consistency objective jointly with landmark alignment. To further preserve local surface structure and enforce topological regularity, we introduce geometry-aware constraints based on Gaussian curvature and conformal consistency, along with auxiliary regularizations that correct fine artifacts such as lip seams and eyelid discontinuities. Our hierarchical optimization with geometry-aware regularization yields meshes with semantically meaningful edge flow and industry-grade topology. After geometry reconstruction, we extract UV-space texture and normal maps to preserve appearance details for visualization and downstream use. In a user study with 22 professional technical artists, our results were assessed as approaching industry-grade usability, and 95% of participants ranked our method as the top-performing approach, underscoring its effectiveness for real-world digital human production.

CCS Concepts: • **Computing methodologies** → **Mesh models.**

Additional Key Words and Phrases: Head Mesh Reconstruction

*The first three authors contributed equally.

Authors' Contact Information: Yunmu Wang; Zoubin Bi; Bowen Cai; Chenchu Rong; Jinlong Wang; Junchen Deng; Aocheng Huang; Jidong Jia; Huan Fu, Alibaba Group, Beijing, China.

Permission to make digital or hard copies of all or part of this work for personal or classroom use is granted without fee provided that copies are not made or distributed for profit or commercial advantage and that copies bear this notice and the full citation on the first page. Copyrights for components of this work owned by others than the author(s) must be honored. Abstracting with credit is permitted. To copy otherwise, or republish, to post on servers or to redistribute to lists, requires prior specific permission and/or a fee. Request permissions from permissions@acm.org.

© 2026 Copyright held by the owner/author(s). Publication rights licensed to ACM. ACM XXXX-XXXX/2026/5-ART
<https://doi.org/10.1145/nnnnnnn.nnnnnnn>

ACM Reference Format:

Yunmu Wang, Zoubin Bi, Bowen Cai, Chenchu Rong, Jinlong Wang, Junchen Deng, Aocheng Huang, Jidong Jia, and Huan Fu. 2026. High-Fidelity Single-Image Head Modeling with Industry-Grade Topology. 1, 1 (May 2026), 11 pages. <https://doi.org/10.1145/nnnnnnn.nnnnnnn>

1 Introduction

High-fidelity head meshes play a central role in many vision and graphics applications, ranging from digital human production to AR/VR and digital twins. In professional film and VFX pipelines, a usable head mesh must satisfy more than visual realism. It should have clean topology, anatomically faithful geometry, and semantically consistent edge flow in critical deformation regions such as the eyelids and lips. It must also be ready for downstream binding with minimal manual cleanup. Producing such assets still depends largely on skilled artists using specialized tools, making the process labor-intensive and often requiring hours or days for each individual head. This manual bottleneck limits scalability and consistency, motivating research on automated, high-quality head modeling.

The central challenge in automating digital head creation lies in generating a topologically consistent mesh that adheres to artist-defined edge layouts while faithfully preserving identity and fine-scale geometry (e.g., wrinkles and eye contours). Existing approaches fall into two main paradigms: 3D Morphable Models (3DMMs) and 3D registration. 3DMMs [Banz and Vetter 2023] offer a compact and controllable representation of facial geometry, enabling stable reconstruction from limited inputs. Although larger datasets and richer basis spaces [Li et al. 2017; Paysan et al. 2009] have improved their capacity, 3DMMs still struggle to reproduce identity-specific nuances and high-frequency realism. Conversely, the scan-to-registration paradigm, which forms the foundation for constructing 3DMM bases, remains the most reliable route for accurately digitizing real individuals. Despite advances in registration algorithms [Vesdapunt et al. 2020; Yang et al. 2023; Zheng et al. 2022], substantial manual refinement by digital artists is still required to correct local artifacts,

particularly around delicate regions such as the eyelids and lips. For subjects that cannot be directly scanned, achieving a high-fidelity, cleanly organized head mesh remains an open challenge—even with the advent of large-scale generative models [Hong et al. 2023; Wang et al. 2025; Zhang et al. 2024].

In this work, we present an automatic optimization framework that reconstructs high-fidelity, industry-grade head meshes from a single facial image and can be instantiated on different rigged templates. Our method deforms a standardized, rigged facial template in a coarse-to-fine manner—optimizing successively at the global rig, joint, and vertex levels—to progressively introduce semantically meaningful deformations, which enhance geometric accuracy while preserving clean topology. The deformation process is driven by two key cues derived from the input image: a predicted normal map and 2D facial landmarks. Normals provide strong local geometric guidance and are less ambiguous than depth estimates in monocular settings. We tailor landmark supervision to different feature types: Mean Squared Error (MSE) loss for sparse corner points (eyes, mouth) and Chamfer Distance (CD) for dense contours (eye shapes), which better preserves their respective geometric properties. However, these cues alone can distort mesh quality and fine-scale topology. We therefore regularize the optimization with Gaussian curvature, which preserves intrinsic surface smoothness, and a conformal constraint that prevents local angular distortions. Additional lightweight priors are applied to correct subtle yet perceptually important defects such as lip seams and eyelid discontinuities. Following geometry reconstruction, we capture texture and normal maps in UV space, while reusing the remaining material maps from the template to assemble the final digital head. The extraction procedure is straightforward, involving intrinsic decomposition, gradient-based normal computation, and Dual-Mask Poisson Blending.

Extensive experiments demonstrate that our method generates identity-preserving head meshes with clean, artist-defined topology. It achieves an ArcFace cosine similarity of 0.3770 and a geometric RMSE of 0.0159 , outperforming state-of-the-art single-image reconstruction approaches. Despite relying on only a single input image, our method attains geometric accuracy comparable to recent scan-based registration methods in our controlled evaluation. In a user study with 22 professional technical artists, participants rated our topology as nearing industry-grade usability, and 95% ranked our method as the top-performing approach. Together, these findings support the use of our reconstructions in downstream binding workflows and subsequent animation tests.

2 Related Work

2.1 Reconstruction

Parametric models. Reconstructing 3D faces from limited observations is inherently ill-posed, as multiple shapes may correspond to the same 2D projection. Parametric methods address this ambiguity by constraining the solution within a low-dimensional latent space learned from 3D scans, imposing strong statistical priors on geometry and appearance. The 3D Morphable Model (3DMM) [Blanz and Vetter 2023] represents shape and texture in a PCA space and has since been extended with larger datasets [Booth et al. 2018;

Li et al. 2017; Paysan et al. 2009] or in-the-wild images [Booth et al. 2017; Feng et al. 2021; Kemelmacher-Shlizerman 2013], and further disentangled identity and expression through bilinear formulations [Bolkart and Wuhler 2015; Cao et al. 2013; Vlastic et al. 2006; Yang et al. 2020]. Recent 3DMM variants [Chai et al. 2022; Li et al. 2017; Ploumpis et al. 2019; Xu et al. 2020; Yang et al. 2020] provide richer control over pose and expression but remain limited by their linear subspaces, which fail to capture fine geometric variations. To increase flexibility, non-linear and hierarchical latent models [Bouritsas et al. 2019; Dib et al. 2024; Giebenhain et al. 2023; Ranjan et al. 2018; Tran and Liu 2018; Zheng et al. 2022] leverage deep architectures to learn complex shape manifolds. However, their capacity is still bounded by available high-quality scan data, which are costly to acquire. Several works [Feng et al. 2021; Lei et al. 2023; Wang et al. 2022] enhance local fidelity by predicting displacement or normal maps, though these may distort mesh regularity and degrade deformation consistency. Rendering-based approaches such as MICA [Zielonka et al. 2022] use inverse-rendering supervision but remain sensitive to lighting ambiguities. SMIRK [Retsinas et al. 2024] alleviates this by replacing differentiable rendering with neural synthesis for more faithful expressions. Recent formulations, e.g., FlowFace [Taubner et al. 2024] and Pixel3DMM [Giebenhain et al. 2025], directly predict UV-space flow fields or dense normal maps for higher-frequency refinement. Overall, parametric models ensure stable, semantically interpretable reconstruction but sacrifice local expressiveness. Our method mitigates this trade-off through hierarchical optimization that maintains topological regularity while recovering fine-scale details.

Non-parametric models. In contrast, non-parametric methods directly infer 3D geometry—via vertex positions, depth, or implicit fields—allowing more flexible, high-fidelity reconstruction. Classical multi-view stereo (MVS) systems [Beeler et al. 2011; Ghosh et al. 2011; Ma et al. 2007] achieve accurate geometry but are computationally heavy and rely on controlled setups. Recent volumetric methods [Bolkart et al. 2023; Li et al. 2021] predict faces in feature volumes for parameter-free, near-real-time inference, though their tessellation irregularity limits animation. Single-image regressors [Richardson et al. 2017; Sela et al. 2017; Zeng et al. 2019] remove multi-view dependency but often overfit, yielding artifacts or inconsistent surfaces. The advent of neural implicit representations [Bi et al. 2024; Chan et al. 2022; Kerbl et al. 2023; Mildenhall et al. 2021; Wang et al. 2021; Zhang et al. 2023b] and large-scale generative architectures [Ho et al. 2020; Lipman et al. 2022; Peebles and Xie 2023; Vaswani et al. 2017; Wang et al. 2025] has enabled impressive 3D reconstruction and synthesis [Chen et al. 2025; Chu and Harada 2024; Feng et al. 2025; Hong et al. 2023; Lai et al. 2025; Li et al. 2025; Qiu et al. 2025; Wang et al. 2023; Wu et al. 2025; Xiang et al. 2025; Zhang et al. 2024]. Despite their realism, these models usually output volumetric or point-based representations requiring post-processing to extract meshes, leading to inconsistent topology across subjects. Such inconsistency impedes rigging, animation, and semantic editing. While non-parametric methods excel in visual fidelity, they remain unsuitable for reconstructing industry-grade head meshes with stable topology for downstream binding and animation workflows. Our framework combines the stability of parametric modeling with the geometric precision of non-parametric

approaches, producing consistent, high-fidelity head meshes from monocular input.

2.2 Registration

Registration aims to deform a template mesh to align with a scan or another irregular yet accurate mesh, producing high-detail surfaces with regular topology for animation and statistical modeling. Classical non-rigid ICP methods optimize vertex transformations under local rigidity or smoothness priors [Allen et al. 2003; Amberg et al. 2007; Sorkine and Alexa 2007], while extensions incorporate conformal [Yoshiyasu et al. 2014] or curvature-based [Tajdari et al. 2022] regularization to preserve local shape characteristics. Our approach similarly enforces conformality and curvature consistency but unifies them within a single optimization framework for locally faithful deformation. Thin-plate spline (TPS) formulations [Bookstein 2002; Chui and Rangarajan 2000] and Coherent Point Drift (CPD) [Myronenko and Song 2010] provide alternative probabilistic or smooth functional mappings, though they remain computationally expensive or prone to underfitting in complex cases. Gaussian Process Morphable Models (GPMs) [Lüthi et al. 2017] generalize deformation priors within a probabilistic framework, later extended by adaptive skinning models (ASM) [Yang et al. 2023] for improved accuracy with compact parameters. Hierarchical strategies [Cheng et al. 2017; Dai et al. 2018; Pears et al. 2023] improve convergence but typically rely on naive local scaling. In contrast, our hierarchical parameterization leverages semantic structure for intuitive multi-level control. More recent neural approaches, such as JNR [Vesdapunt et al. 2020] and SPHEAR [Bazavan et al. 2024], learn compact neural representations or spherical embeddings to achieve efficient feedforward registration. While registration-based pipelines rely on precise scan data and often require manual artifact correction, our method reduces this acquisition burden by reconstructing industry-grade head meshes from a single image, streamlining mesh creation for production workflows.

3 Preliminary

Rigged Template. We define a rigged template for a target mesh topology as $\mathcal{T} = (\bar{\mathbf{V}}, \mathcal{F}, \mathcal{R}, \mathcal{J}, \bar{\boldsymbol{\theta}}, \mathbf{W}, \Delta)$, where $\bar{\mathbf{V}} \in \mathbb{R}^{N \times 3}$ denotes the neutral vertex positions, \mathcal{F} is the fixed mesh connectivity, \mathcal{R} is the set of rig controllers, \mathcal{J} is the joint hierarchy, $\bar{\boldsymbol{\theta}}$ denotes the default local joint parameters, \mathbf{W} contains the skinning weights, and Δ denotes residual vertex offsets. A different target topology requires a corresponding rigged template defined under the same representation.

Following JNR [Vesdapunt et al. 2020], ASM [Yang et al. 2023], and related rigged face models, each joint $j_k \in \mathcal{J}$ is associated with a local transform relative to its parent in the hierarchy. In addition to the joint layer, our template contains a controller layer \mathcal{R} , similar in spirit to production facial rigs such as MetaHuman [Epic Games 2021]. Each controller $r_i \in \mathcal{R}$ is a bounded parameter associated with a semantically meaningful facial deformation. In this work, this rig serves as a reconstruction-time deformation parameterization, rather than the downstream facial rig used for expression animation.

Given a controller vector \mathbf{r} , the local joint parameters are driven by a sparse controller-to-joint mapping, $\boldsymbol{\theta}(\mathbf{r}) = \bar{\boldsymbol{\theta}} + \Phi(\mathbf{r})$, where

$\Phi(\mathbf{r})$ aggregates controller-dependent offsets in joint-parameter space. The corresponding joint transforms are obtained by forward kinematics over the hierarchy. The deformed mesh is then computed by linear blend skinning with residual offsets:

$$\mathbf{V}(\mathbf{r}) = \text{LBS}(\bar{\mathbf{V}}, \mathbf{T}(\boldsymbol{\theta}(\mathbf{r})), \mathbf{W}) + \Delta(\mathbf{r}),$$

where $\mathbf{T}(\boldsymbol{\theta}(\mathbf{r}))$ denotes the hierarchy-consistent joint transforms and $\Delta(\mathbf{r}) \in \mathbb{R}^{N \times 3}$ denotes controller-dependent residual vertex offsets. This formulation defines a three-level deformation hierarchy, consisting of controller values, joint parameters, and vertex positions, which are optimized successively in the following section.

4 Methodology

4.1 Framework

Given the rigged template defined in Sec. 3, our method reconstructs an *industry-grade* head mesh from a *single* image through hierarchical optimization. As illustrated in Fig. 2, we successively optimize rig parameters, joint parameters, and vertex positions, corresponding to global deformation, mid-level articulation, and fine-scale geometric refinement. This coarse-to-fine strategy preserves clean topology and coherent edge flow:

- (1) **Rig-level optimization:** We first optimize the rig parameters, where each controller corresponds to a semantically meaningful facial region (e.g., the jaw, cheeks, or brows). The resulting deformations are propagated along the rig–joint–vertex hierarchy, enabling expressive and structurally consistent global shape changes.
- (2) **Joint-level optimization:** Next, we fix the rig and optimize the joint parameters, which retain local semantic meaning while offering finer local control. This stage refines mid-level geometry through localized deformations, ensuring a smooth transition from rig-driven deformation to dense surface reconstruction.
- (3) **Vertex-level optimization:** Finally, we directly optimize vertex positions to recover fine-scale surface details such as wrinkles and subtle skin folds, achieving high-fidelity reconstruction.

By progressively refining from semantic to fine-scale deformations, our hierarchical optimization produces meshes that preserve individual identity comparable to registration-based methods while maintaining more coherent edge flow, achieving this high-fidelity reconstruction from only a single input image.

4.2 Shape Reconstruction

We illustrate our formulation using rig-level optimization as an example; the same objective generalizes across all three parameter levels, differing only in the optimized variables and hyperparameters. Given a *single* input facial image I and a rigged template \mathcal{T} defined in Sec. 3, we optimize the current parameter level to reconstruct the input identity while preserving topological consistency. The resulting mesh is evaluated through differentiable rendering with the unified objective $\mathcal{L} = \mathcal{L}_{\text{id}} + \mathcal{L}_{\text{con}} + \mathcal{L}_{\text{reg}}$, where \mathcal{L}_{id} , \mathcal{L}_{con} , and \mathcal{L}_{reg} denote the identity, topological consistency, and regularization losses, respectively.

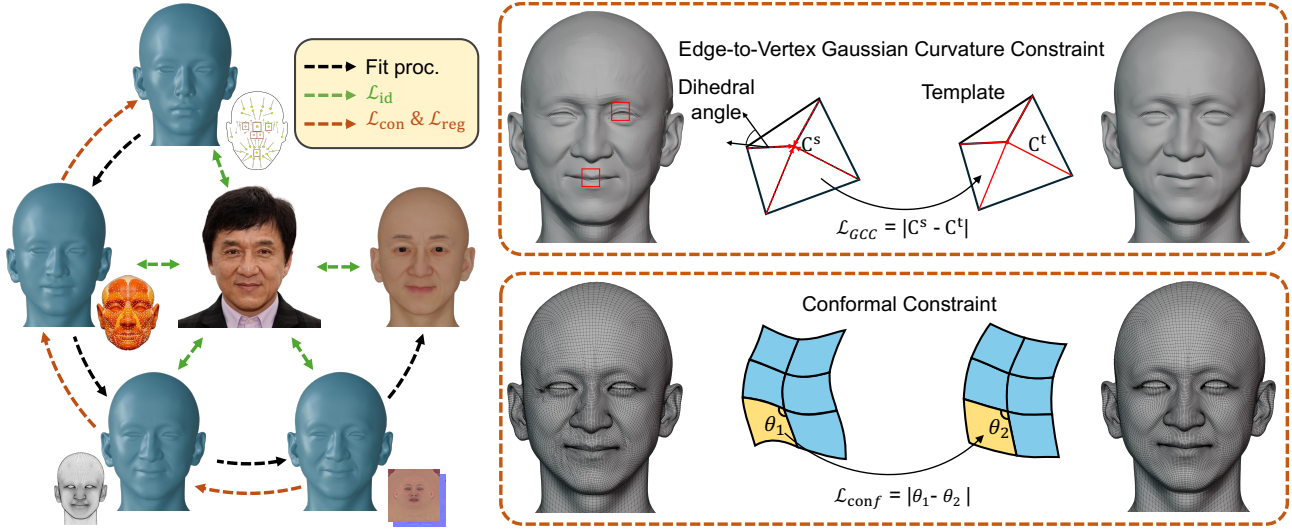


Fig. 2. **Overview of our pipeline.** **Left:** Our method adopts a coarse-to-fine reconstruction framework that hierarchically deforms the template mesh from semantic structure to fine-scale details, yielding semantically meaningful edge flow and industry-grade topology. **Right:** We introduce Gaussian curvature and conformal consistency losses to simultaneously preserve local surface geometry and enforce topological regularity.

In the following, we first introduce the primary supervision signals—normal and facial landmark constraints—that drive identity reconstruction (Sec. 4.2.1). We then present Edge-to-Vertex Gaussian Curvature and conformal constraints that enforce topological consistency (Sec. 4.2.2). Finally, we describe additional regularization terms that address subtle yet critical artifacts (Sec. 4.2.3).

4.2.1 Facial Identity Restoration. To preserve high-frequency geometric details while mitigating the inherent ill-posedness of monocular 3D face reconstruction, our method integrates two complementary supervision signals: $\mathcal{L}_{id} = \lambda_n \mathcal{L}_n + \lambda_{land} \mathcal{L}_{land}$, where \mathcal{L}_n and \mathcal{L}_{land} denote the normal and landmark supervision terms, and $\lambda_n, \lambda_{land}$ are their respective weights. Normal supervision provides dense, local geometric cues that are more robust than direct 3D supervision and capture perceptually critical fine-scale features such as wrinkles and subtle curvature variations. In contrast, landmark supervision enforces semantic alignment by anchoring key structural regions—eyes, mouth, and facial contour—thus stabilizing global shape and promoting coherent edge flow during optimization. For normal prediction, we adopt the base model of Garcia et al. [Garcia et al. 2025] and fine-tune it with an additional 100K synthetic samples to enhance local fidelity and normal consistency. For landmark detection, we employ an RTMPose-style network [Jiang et al. 2023] comprising a CSPNeXt backbone [Lyu et al. 2022] and SimCC head [Li et al. 2022], trained on 100K synthetic renderings and 50K FFHQ [Karras et al. 2019] images. Training configurations and additional implementation details are provided in our supplementary material.

Normal Consistency. To ensure that the reconstructed mesh preserves high-frequency geometric features that are critical to identity, we introduce an ℓ_1 normal consistency loss: $\mathcal{L}_n = \|\mathcal{N}(I) - \hat{\mathcal{N}}(V)\|_1$, where $\mathcal{N}(I)$ denotes the per-pixel surface normals predicted from the input image, and $\hat{\mathcal{N}}(V)$ represents the rendered surface normals computed from the current 3D mesh with vertices V . Supervising

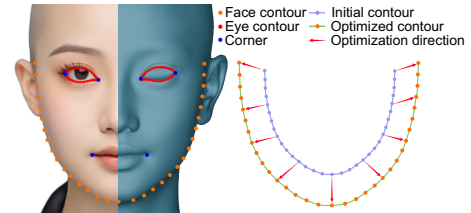


Fig. 3. **Definition of our landmarks.** Besides classic corner landmarks, we introduce sequential point trajectories to better guide the reconstruction of identity-relevant features, such as eye shape and overall face contour.

reconstruction with surface normals provides a rich geometric signal beyond classic point-wise correspondence, enabling the model to better capture identity-specific local curvature and fine-scale shape variations. This normal alignment encourages high-fidelity reproduction of individual facial structures, which is essential for faithful identity modeling.

Landmark Alignment. As shown in Fig. 3, our landmark set includes (1) corner points of the eyes and mouth and (2) sequential landmarks along the eye and facial contours. The corner points provide sparse yet reliable anchors that constrain the global scale and orientation of the reconstruction, and their alignment is measured by a Mean Squared Error (MSE) loss. The contour landmarks offer denser supervision for capturing local geometric details and boundary consistency. Because the number of detected landmarks and projected mesh vertices along the contours may differ, we measure their correspondence using a one-sided Chamfer distance.

The overall landmark alignment loss is defined as:

$$\mathcal{L}_{land} = \frac{1}{N_c} \sum_{i=1}^{N_c} \|\hat{\mathbf{u}}_i - \mathbf{u}_i\|_2^2 + \frac{1}{|\hat{U}|} \sum_{\hat{\mathbf{u}} \in \hat{U}} \min_{\mathbf{u} \in U} \|\hat{\mathbf{u}} - \mathbf{u}\|_2^2, \quad (1)$$

where N_c is the number of corner points, $\hat{\mathbf{u}}_i$ and \mathbf{u}_i are the projected and detected 2D coordinates of the i -th corner, and \hat{U} and U denote the sets of projected and detected contour landmarks.

4.2.2 Topological Consistency Enforcement. Normal and landmark losses preserve global identity but often produce locally inconsistent mesh structures, which are unsuitable for industry-grade head meshes. To ensure geometric plausibility during deformation, we introduce two complementary topological consistency constraints: $\mathcal{L}_{\text{con}} = \lambda_{\text{GCC}} \mathcal{L}_{\text{GCC}} + \lambda_{\text{conf}} \mathcal{L}_{\text{conf}}$, where \mathcal{L}_{GCC} enforces curvature consistency and $\mathcal{L}_{\text{conf}}$ encourages local angle preservation. Together, these terms maintain intrinsic surface properties and suppress non-physical distortions during optimization.

Edge-to-Vertex Gaussian Curvature Constraint (EV-GCC). Gaussian curvature constraints are commonly used in mesh deformation [Meyer et al. 2003; Tajdari et al. 2022] to preserve intrinsic geometry. However, vertex-based curvature computed via angle deficits suffers from irregular neighborhoods and poor parallelization, while edge-based dihedral-angle formulations are difficult to integrate with vertex-level supervision in differentiable frameworks. To reconcile these trade-offs, we introduce an edge-to-vertex curvature formulation that redistributes edge-level dihedral angles to adjacent vertices using normalized weights. This enables vertex-level curvature supervision while preserving the locality and efficiency of edge-based processing. For each edge e_{ij} , the dihedral angle is computed as $\theta_{ij}^e = \arccos(\mathbf{n}_1 \cdot \mathbf{n}_2)$,

where \mathbf{n}_1 and \mathbf{n}_2 denote the normals of the adjacent faces sharing e_{ij} . The curvature at vertex i is accumulated as

$$c_i = \sum_{j=1}^{n_{c_i}} \omega_{i \rightarrow ij} \theta_{ij}^e, \quad \omega_{i \rightarrow ij} = \frac{I_{i \rightarrow ij}}{\sum_k I_{i \rightarrow ik}}, \quad (2)$$

where $I_{i \rightarrow ij}$ represents the importance weight of edge e_{ij} . The curvature consistency loss is defined as $\mathcal{L}_{\text{GCC}} = \sum_{i=1}^{N_v} |c_i^s - c_i^t|$, with c_i^s and c_i^t denoting curvature values at vertex i on the source and target meshes, respectively.

Angle Preservation Constraint. We further enforce local conformality using an angle-preservation term inspired by mesh parameterization and UV unwrapping [Gu and Yau 2003; Lévy et al. 2023; Yoshidasu et al. 2014]. This constraint penalizes deviations between corresponding internal triangle angles: $\mathcal{L}_{\text{conf}} = \sum_{i \in \Omega_\theta} \|\theta_i^s - \theta_i^t\|$, where θ_i^s and θ_i^t denote the internal angles at the i -th triangle corner in the source and target meshes. To prioritize regions undergoing large deformations, we rank the angular discrepancies and retain the top Ω_θ entries for loss computation.

Together, EV-GCC and conformal constraints enforce topological coherence and geometric realism, significantly improving surface stability under large facial deformations.

4.2.3 Fine Artifacts Suppression. While topological consistency constraints preserve intrinsic geometry and surface regularity, subtle artifacts can persist in visually sensitive regions (e.g., lips and eyes) due to high deformability. We therefore introduce fine-level regularization to enforce local orientation, contour smoothness, and optimization stability:

$$\mathcal{L}_{\text{reg}} = \lambda_{\text{flip}} \mathcal{L}_{\text{flip}} + \lambda_{\text{curve}} \mathcal{L}_{\text{curve}} + \lambda_{\text{disp}} \mathcal{L}_{\text{disp}}, \quad (3)$$

where $\mathcal{L}_{\text{flip}}$ prevents normal flipping, $\mathcal{L}_{\text{curve}}$ smooths eyeline contours, and $\mathcal{L}_{\text{disp}}$ stabilizes vertex displacements.

Face-Flip Constraint. Flipping artifacts in highly deformable facial regions such as the lips and oral cavity can produce visually implausible shading and animation artifacts. To suppress such effects, we introduce a normal regularization that penalizes large deviations in face orientations between corresponding source and target meshes: $\mathcal{L}_{\text{flip}} = \sum_{i \in \Omega_{\vec{n}}} \|\vec{n}_i^s - \vec{n}_i^t\|$, where \vec{n}_i^s and \vec{n}_i^t denote the unit normals of the i -th face in the source and target meshes. Similar to $\mathcal{L}_{\text{conf}}$, the top $\Omega_{\vec{n}}$ faces with the largest normal deviations are selected to focus supervision on regions most prone to inversion. This constraint preserves consistent surface orientation and suppresses normal flips that disrupt local topology.

Eyeline Curve Flow Constraint. The eyes are among the most perceptually critical facial regions, yet their fine geometric structures often lead to jagged contours during deformation. We introduce a weak regularizer that promotes smooth directional flow along key curves (e.g., the upper eyelid crease and outer eye contour) while remaining tolerant to subject-specific variations. As an example, for the upper eye outline defined by an ordered vertex sequence $\{v_1, \dots, v_n\}$, we compute local direction vectors:

$$\vec{d}_i = \frac{1}{2} \left(\frac{\vec{v}_{i+1} - \vec{v}_i}{\|\vec{v}_{i+1} - \vec{v}_i\|} + \frac{\vec{v}_{i+2} - \vec{v}_{i+1}}{\|\vec{v}_{i+2} - \vec{v}_{i+1}\|} \right), \quad (4)$$

for $i = 1, \dots, n - 2$. The turning smoothness feature is then defined as the normalized angle change between consecutive directions:

$$f_i = \frac{1}{\|\vec{v}_{i+1} - \vec{v}_i\|} \arccos \left(\frac{\vec{d}_i \cdot \vec{d}_{i+1}}{\|\vec{d}_i\| \|\vec{d}_{i+1}\|} \right). \quad (5)$$

We measure the ℓ_1 discrepancy between the flow features of the source and target curves: $\mathcal{L}_{\text{curve}} = \sum_{i=1}^{n-3} |f_i^s - f_i^t|$. This term enforces smooth curvature transitions along delicate contours, suppressing unnatural jaggedness around the eyes.

Vertex Displacement Regularization. We further impose a regularization on vertex displacements $\mathcal{L}_{\text{disp}} = \sum_{i=1}^{N_v} \|\Delta \mathbf{v}_i\|$ to stabilize the deformation optimization process. This term mitigates cumulative geometric drift by encouraging smooth shape evolution, resulting in more stable convergence and fewer local artifacts.

4.3 Texture Extraction

Following geometry reconstruction, we generate appearance maps via a UV-space texture pipeline as illustrated in Fig. 4. To bridge the resolution gap between the input image and the target UV map, we first upsample the input using a Real-ESRGAN-based super-resolution module [Wang et al. 2021]. Subsequently, we employ an intrinsic decomposition model [Liang et al. 2025] to extract the albedo, effectively decoupling shading effects while preserving fine-grained details. Meanwhile, a heuristic normal map is generated in the image space. Both the albedo and the normal map are projected directly onto the UV space. Unlike per-vertex color baking, this rasterization strategy preserves high-frequency details. Finally, to address missing regions caused by self-occlusion, we utilize the Dual-Mask Poisson Blending method to inpaint the texture, ensuring gradient consistency and color coherence in the final UV map. We highlight two components that deviate from conventional pipelines:

Normal Computation. Neural network–predicted normals often suffer from scale ambiguity and overly smoothed high-frequency details. To address this, we adopt a gradient-based strategy [Ratz 2017]. Specifically, the Sobel operator is applied to both fine- and coarse-resolution facial images to compute horizontal and vertical gradients ($g_{i,j}^x, g_{i,j}^y$). The tangent-space normal is defined as $\mathbf{n}_{i,j} \propto (g_{i,j}^x, g_{i,j}^y, 1)$. The two normal maps are then fused using a soft-light operation, which preserves high-frequency geometric cues while maintaining smooth global structure, resulting in stable and detailed surface normals.

Dual-Mask Poisson Blending. Since single-view texture predictions are inherently incomplete due to occlusions, we complete them by blending with template textures $\tilde{\mathcal{A}}$. To avoid artifacts and tone shifts that arise from direct Poisson blending, we employ a dual-mask blending scheme. A soft parsing mask guides smooth transitions in interior regions, while a hard boundary mask preserves precise seam constraints. We derive the hard mask directly from a facial parsing map [Yakhyyokhuja 2024] and generate the soft mask by applying a 3×3 erosion kernel. This dual-mask approach produces seamless transitions while maintaining consistent global appearance throughout the UV map.

5 Experiments

5.1 Experimental settings

Settings. In the main quantitative experiments, we use a rigged template following the MetaHuman mesh topology [Epic Games 2021] for illustration. The template comprises 24,049 vertices, 808 joints, and 147 rig controllers, supporting high-fidelity geometric deformation. We implement our method in PyTorch [Paszke et al. 2019] and use the differentiable rasterizer from PyTorch3D [Ravi et al. 2020]. Optimization hyperparameters and learning-rate schedules are provided in the supplementary material. All experiments are performed on a workstation with an NVIDIA Tesla V100 (32 GB) GPU; CPU-only runs use an Intel Xeon Platinum 8163 processor. On this hardware, our full pipeline takes about 4.5 minutes per input image, including 2.5 minutes for geometry reconstruction and 2 minutes for texture extraction. Our reconstruction assumes a near-neutral, unoccluded face image. For samples with large pose or significant occlusion, we first apply a fine-tuned FLUX.1 Kontext [Labs et al. 2025] preprocessing model to frontalize the face and remove major occluders, as shown in the inset of Fig. 1. This preprocessing is used only to satisfy the input assumption; when it is needed, we apply the same preprocessed input to all compared methods for fairness. Additional preprocessing details are provided in the supplementary material.

Baselines. We compare our method against widely used single-image face reconstruction methods and classical mesh registration approaches. For reconstruction, we include FaceScape [Yang et al. 2020], DECA [Zielonka et al. 2022], MICA [Zielonka et al. 2022], and Pixel3DMM [Giebenhain et al. 2025], all of which rely on low-dimensional parametric spaces (e.g., FaceScape or FLAME [Li et al. 2017] shape bases) and output relatively low-resolution meshes. For registration baselines, we evaluate NR-ICP [Amberg et al. 2007] and ACAP [Yoshiyasu et al. 2014] under the same template topology, and include FLAME as a representative parametric registration method.

Method	Synthetic				In-the-wild
	RMSE ↓	NC ↑	ArcFace ↑	ArcFace* ↑	ArcFace ↑
FaceScape	0.0318	0.9609	0.1765	0.3173	0.1341
DECA	0.0402	0.9706	0.1834	0.4359	0.1014
MICA	0.0474	0.9711	0.1621	0.3980	0.1213
Pixel3DMM	0.0630	0.9704	0.1876	0.4332	0.1472
Ours	0.0159	0.9798	0.3770	0.6322	0.4140

Table 1. **Comparison of single-image head reconstruction methods on Synthetic and In-the-wild datasets.** * denotes the ArcFace score computed on ground-truth renderings under the same camera, lighting, and diffuse gray material.

Method	RMSE ↓	NC ↑	ArcFace ↑	ArcFace* ↑
FLAME	0.0215	0.9755	0.2192	0.4915
NR-ICP	0.0013	0.9944	0.4196	0.8196
ACAP	0.0028	0.9910	0.3654	0.6793
Ours	0.0019	0.9975	0.4397	0.9421

Table 2. **Comparison with 3D face registration methods.** * denotes the ArcFace score computed on ground-truth renderings under the same camera, lighting, and diffuse gray material.

Datasets. Our experiments are evaluated on two datasets. To ensure access to accurate ground truth, we construct a synthetic dataset by combining 66 publicly available head models [Epic Games 2021] with 40 artist-created high-quality assets. In addition, we collect 158 in-the-wild images from public web sources, academic datasets [Karras et al. 2019; Liu et al. 2015], and image generation tools, covering a wide variety of conditions and styles. These evaluation images span diverse human subjects across skin tones, as well as non-photorealistic domains such as anime characters. This data composition supports broad qualitative and quantitative evaluation of our method.

Evaluation Metrics. We evaluate our method using standard geometric metrics, including Root Mean Square Error (RMSE) and Normal Consistency (NC), as well as ArcFace similarity, which measures identity preservation—an aspect that is often more important than pure geometric accuracy for face reconstruction, since faithful identity retention is essential for downstream binding and animation workflows. For a fair comparison of identity preservation, we render all reconstructed heads using PyTorch3D under the same front-view camera, material, and lighting configuration, and compute the ArcFace [Deng et al. 2019] cosine similarity between the rendered images and the input image. To ensure fair geometric comparison across all methods, we uniformly resample all meshes to a fixed number of points and evaluate errors within a masked facial region. Further implementation details for the metric computation are provided in the supplementary material.

5.2 Results

As shown in Fig. 1 and Fig. 11, our method produces high-fidelity 3D reconstructions with strong identity preservation, faithfully recovering person-specific geometric structure. The reconstructed meshes also exhibit stable behavior after downstream binding in

animation tests while maintaining identity consistency. We further validate our framework on two different head-mesh topologies in Fig. 9 and obtain industry-grade reconstructions with strong identity preservation in both settings. The consistent behavior across these topology configurations provides empirical support that our method is not tied to a specific template topology. Beyond these qualitative observations, we evaluate our approach through quantitative and qualitative comparisons against recent state-of-the-art methods.

Single-image Face Reconstruction. We assess our method on both synthetic renderings and in-the-wild images. On synthetic data, we compare against representative 3DMM-based models, including FaceScape, DECA, MICA, and Pixel3DMM. As shown in Fig. 5, among existing parametric models only FaceScape produces roughly comparable facial proportions, but its limited shape space often introduces noticeable artifacts, such as overly pronounced brow ridges and jawlines. In contrast, our method achieves accurate, stable reconstruction with substantially better identity retention, reflected by significantly higher ArcFace cosine similarity scores in Tab. 1. To evaluate generalization, we conduct experiments on in-the-wild images. Our method consistently outperforms all baselines across diverse lighting, pose, and appearance conditions. The ArcFace similarity distributions in Fig. 7 further show that our reconstructed identities remain more faithful, even under uncontrolled imaging conditions.

Comparison with DreamFace [Zhang et al. 2023a]. Since DreamFace is closed-source and does not provide a batch API, we report ArcFace measurements only on our in-the-wild dataset. Using the official web interface provided by [Deemos 2023], DreamFace achieves an ArcFace score of 0.1821 , whereas our method reaches 0.4140 . As shown in Fig. 10, DreamFace preserves identity less faithfully, often failing to recover fine-grained facial details and, in some cases, even struggling to reproduce the coarse facial structure (e.g., rows 3 and 4). In contrast, our method reliably reconstructs both the global facial geometry and subtle high-frequency cues, including fine surface details such as wrinkles.

Scan-to-fitting Face Registration. We also compare our fitting accuracy with classical optimization-based registration methods (NR-ICP and ACAP) and the parametric FLAME model. For this controlled comparison, our method uses rendered normals as input, whereas the other methods directly utilize the ground-truth model. Unlike learned registration baselines that require scan datasets for model fitting, our optimization stage does not require subject-specific scan training data. As illustrated in Fig. 6, our method surpasses FLAME in 3D fitting accuracy while maintaining semantic consistency and producing clean, regular topology. Quantitative results reported in Tab. 2 show that our method reaches accuracy comparable to classical optimization-based techniques while operating from only a *single* input image. It preserves individual identity more faithfully and produces coherent edge flows, highlighting both the effectiveness and the generality of our registration design.

Downstream Application. We further evaluate the usability of the reconstructed heads in downstream facial animation workflows. For this test, each reconstructed mesh is bound to an independent facial rig that is not used during reconstruction. As shown in Fig. 11, our meshes maintain consistent topology and semantically aligned edge

flow, enabling integration with standard facial rigs and expression controllers after binding. When driven by skeleton-based animation, the meshes deform smoothly and stably across large expressions and extreme poses in our test sequences, while preserving local details such as wrinkles and skin folds. We observe no visible tearing or texture distortion in the shown motion sequences. These results suggest that our method produces industry-grade head meshes well suited for downstream binding and animation.

5.3 Ablations

We conduct ablation studies to analyze the contribution of each key component in our optimization framework. As shown in Fig. 2 and Fig. 8, removing any of these terms leads to noticeable degradation in geometric fidelity, surface smoothness, or topological regularity. **Edge-to-Vertex Gaussian Curvature Constraint** mitigates surface artifacts caused by local optimization minima by enforcing curvature consistency with the standardized mesh. Without EV-GCC, the reconstructed surfaces exhibit high-frequency noise and irregular shading, as shown in the second column, indicating reduced geometric smoothness and local instability.

Conformal Constraint encourages locally smooth and consistent edge flows across the surface. When this term is removed, the edge orientations become irregular and lose global coherence, resulting in disrupted edge flow patterns and degraded surface regularity, as illustrated in the third column.

Coarse-to-Fine Optimization Framework provides stable initialization and progressively refines details, preventing the optimization from being trapped in suboptimal minima. Directly optimizing vertex positions in a single stage leads to unstable convergence, degraded geometry, and irregular topology that is unsuitable for downstream applications, as demonstrated in the last column.

5.4 User Study

We conducted a user study to assess perceptual quality in terms of global geometric fidelity, mesh layout usability, and overall preference. 22 professional technical artists evaluated 30 reconstructed faces produced by MICA, Pixel3DMM, and our method. On a five-point scale, our method achieved an average score of 3.6, substantially higher than Pixel3DMM (1.6) and MICA (1.42). On the three-point topology-usability scale, our method obtained a score of 1.79, approaching industry-grade usability, whereas Pixel3DMM and MICA scored only 0.31 and 0.34. Overall, 95% of participants ranked our method as the top-performing approach. These results indicate that our meshes achieve both stronger perceptual alignment and more regular edge flow, making them well-suited for downstream binding and animation workflows. Additional details are provided in the supplementary material.

6 Conclusion and Future Work

We present a framework for automatic head mesh reconstruction from a single image. Our method produces highly identity-preserving head geometry while maintaining semantically meaningful, industry-grade edge flow and topology, making the reconstructed meshes suitable for downstream binding workflows. Despite these advantages, our current focus is primarily on geometric reconstruction.

Material modeling and appearance fidelity remain important directions for production-quality digital humans.

Acknowledgments

We thank Kun Yang and all professional artists for their valuable contributions to this project.

References

- Brett Allen, Brian Curless, and Zoran Popović. 2003. The space of human body shapes: reconstruction and parameterization from range scans. *ACM transactions on graphics (TOG)* 22, 3 (2003), 587–594.
- Brian Amberg, Sami Romdhani, and Thomas Vetter. 2007. Optimal step nonrigid ICP algorithms for surface registration. In *2007 IEEE conference on computer vision and pattern recognition*. IEEE, 1–8.
- Eduard Gabriel Bazavan, Andrei Zanfir, Teodor Alexandru Szente, Mihai Zanfir, Thiemo Alldieck, and Cristian Sminchisescu. 2024. SPHEAR: Spherical Head Registration for Complete Statistical 3D Modeling. In *2024 International Conference on 3D Vision (3DV)*. IEEE, 213–224.
- Thabo Beeler, Fabian Hahn, Derek Bradley, Bernd Bickel, Paul A Beardsley, Craig Gotsman, Robert W Sumner, and Markus H Gross. 2011. High-quality passive facial performance capture using anchor frames. *ACM Trans. Graph.* 30, 4 (2011), 75.
- Zoubin Bi, Yixin Zeng, Chong Zeng, Fan Pei, Xiang Feng, Kun Zhou, and Hongzhi Wu. 2024. Gs3: Efficient relighting with triple gaussian splatting. In *SIGGRAPH Asia 2024 Conference Papers*. 1–12.
- Volker Blanz and Thomas Vetter. 2023. A morphable model for the synthesis of 3D faces. In *Seminal Graphics Papers: Pushing the Boundaries, Volume 2*. 157–164.
- Timo Bolkart, Tianye Li, and Michael J Black. 2023. Instant multi-view head capture through learnable registration. In *Proceedings of the IEEE/CVF Conference on Computer Vision and Pattern Recognition*. 768–779.
- Timo Bolkart and Stefanie Wuhrer. 2015. A groupwise multilinear correspondence optimization for 3d faces. In *Proceedings of the IEEE international conference on computer vision*. 3604–3612.
- Fred L. Bookstein. 2002. Principal warps: Thin-plate splines and the decomposition of deformations. *IEEE Transactions on pattern analysis and machine intelligence* 11, 6 (2002), 567–585.
- James Booth, Epameinondas Antonakos, Stylianos Ploumpis, George Trigeorgis, Yannis Panagakis, and Stefanos Zafeiriou. 2017. 3d face morphable models" in-the-wild". In *Proceedings of the IEEE conference on computer vision and pattern recognition*. 48–57.
- James Booth, Anastasios Roussos, Allan Ponniah, David Dunaway, and Stefanos Zafeiriou. 2018. Large scale 3D morphable models. *International Journal of Computer Vision* 126, 2 (2018), 233–254.
- Giorgos Bouritsas, Sergiy Bokhnyak, Stylianos Ploumpis, Michael Bronstein, and Stefanos Zafeiriou. 2019. Neural 3d morphable models: Spiral convolutional networks for 3d shape representation learning and generation. In *Proceedings of the IEEE/CVF international conference on computer vision*. 7213–7222.
- Chen Cao, Yanlin Weng, Shun Zhou, Yiying Tong, and Kun Zhou. 2013. Facewarehouse: A 3d facial expression database for visual computing. *IEEE Transactions on Visualization and Computer Graphics* 20, 3 (2013), 413–425.
- Zenghao Chai, Haoxian Zhang, Jing Ren, Di Kang, Zhengzhuo Xu, Xuefei Zhe, Chun Yuan, and Linchao Bao. 2022. Realy: Rethinking the evaluation of 3d face reconstruction. In *European conference on computer vision*. Springer, 74–92.
- Eric R Chan, Connor Z Lin, Matthew A Chan, Koki Nagano, Boxiao Pan, Shalini De Mello, Orazio Gallo, Leonidas J Guibas, Jonathan Tremblay, Sameh Khamis, et al. 2022. Efficient geometry-aware 3d generative adversarial networks. In *Proceedings of the IEEE/CVF conference on computer vision and pattern recognition*. 16123–16133.
- Xiyi Chen, Shaofei Wang, Marko Mihajlovic, Taewon Kang, Sergey Prokudin, and Ming Lin. 2025. HART: Human Aligned Reconstruction Transformer. *arXiv preprint arXiv:2509.26621* (2025).
- Shiyang Cheng, Ioannis Marras, Stefanos Zafeiriou, and Maja Pantic. 2017. Statistical non-rigid ICP algorithm and its application to 3D face alignment. *Image and Vision Computing* 58 (2017), 3–12.
- Xuangeng Chu and Tatsuya Harada. 2024. Generalizable and animatable gaussian head avatar. *Advances in Neural Information Processing Systems* 37 (2024), 57642–57670.
- Haili Chui and Anand Rangarajan. 2000. A new algorithm for non-rigid point matching. In *Proceedings IEEE Conference on Computer Vision and Pattern Recognition. CVPR 2000 (Cat. No. PR00662)*, Vol. 2. IEEE, 44–51.
- Hang Dai, Nick Pears, and William Smith. 2018. Non-rigid 3D shape registration using an adaptive template. In *Proceedings of the European Conference on Computer Vision (ECCV) Workshops*. 0–0.
- Deemos. 2023. DreamFace. <https://hyper3d.ai/chatavatar>.
- Jiankang Deng, Jia Guo, Niannan Xue, and Stefanos Zafeiriou. 2019. Arcface: Additive angular margin loss for deep face recognition. In *Proceedings of the IEEE/CVF conference on computer vision and pattern recognition*. 4690–4699.
- Abdallah Dib, Luiz Gustavo Hafemann, Emeline Got, Trevor Anderson, Amin Fadaeinejad, Rafael MO Cruz, and Marc-André Carboneau. 2024. MoSAR: Monocular semi-supervised model for avatar reconstruction using differentiable shading. In *Proceedings of the IEEE/CVF Conference on Computer Vision and Pattern Recognition*. 1770–1780.
- Epic Games. 2021. Metahuman Creator. <https://www.unrealengine.com/en-US/metahuman-creator>.
- Xiang Feng, Chang Yu, Zoubin Bi, Yintong Shang, Feng Gao, Hongzhi Wu, Kun Zhou, Chenfanfu Jiang, and Yin Yang. 2025. Arm: Appearance reconstruction model for relightable 3d generation. In *Proceedings of the IEEE/CVF Conference on Computer Vision and Pattern Recognition*. 21425–21437.
- Yao Feng, Haiwen Feng, Michael J Black, and Timo Bolkart. 2021. Learning an animatable detailed 3D face model from in-the-wild images. *ACM Transactions on Graphics (TOG)* 40, 4 (2021), 1–13.
- Gonzalo Martin Garcia, Karim Abou Zeid, Christian Schmidt, Daan De Geus, Alexander Hermans, and Bastian Leibe. 2025. Fine-tuning image-conditional diffusion models is easier than you think. In *2025 IEEE/CVF Winter Conference on Applications of Computer Vision (WACV)*. IEEE, 753–762.
- Abhijeet Ghosh, Graham Fyffe, Borom Tunwattapanong, Jay Busch, Xueming Yu, and Paul Debevec. 2011. Multiview face capture using polarized spherical gradient illumination. In *Proceedings of the 2011 SIGGRAPH Asia Conference*. 1–10.
- Simon Giebenhain, Tobias Kirschstein, Markos Georgopoulos, Martin Rünz, Lourdes Agapito, and Matthias Nießner. 2023. Learning neural parametric head models. In *Proceedings of the IEEE/CVF Conference on Computer Vision and Pattern Recognition*. 21003–21012.
- Simon Giebenhain, Tobias Kirschstein, Martin Rünz, Lourdes Agapito, and Matthias Nießner. 2025. Pixel3DMM: Versatile Screen-Space Priors for Single-Image 3D Face Reconstruction. *arXiv preprint arXiv:2505.00615* (2025).
- Xianfeng Gu and Shing-Tung Yau. 2003. Global conformal surface parameterization. In *Proceedings of the 2003 Eurographics/ACM SIGGRAPH symposium on Geometry processing*. 127–137.
- Jonathan Ho, Ajay Jain, and Pieter Abbeel. 2020. Denoising diffusion probabilistic models. *Advances in neural information processing systems* 33 (2020), 6840–6851.
- Yicong Hong, Kai Zhang, Jiuxiang Gu, Sai Bi, Yang Zhou, Difan Liu, Feng Liu, Kalyan Sunkavalli, Trung Bui, and Hao Tan. 2023. Lrm: Large reconstruction model for single image to 3d. *arXiv preprint arXiv:2311.04400* (2023).
- Tao Jiang, Peng Lu, Li Zhang, Ningsheng Ma, Rui Han, Chengqi Lyu, Yining Li, and Kai Chen. 2023. RtmPose: Real-time multi-person pose estimation based on mmPose. *arXiv preprint arXiv:2303.07399* (2023).
- Tero Karras, Samuli Laine, and Timo Aila. 2019. A style-based generator architecture for generative adversarial networks. In *Proceedings of the IEEE/CVF conference on computer vision and pattern recognition*. 4401–4410.
- Ira Kemelmacher-Shlizerman. 2013. Internet based morphable model. In *Proceedings of the IEEE international conference on computer vision*. 3256–3263.
- Bernhard Kerbl, Georgios Kopanas, Thomas Leimkühler, and George Drettakis. 2023. 3D Gaussian splatting for real-time radiance field rendering. *ACM Trans. Graph.* 42, 4 (2023), 139–1.
- Black Forest Labs, Stephen Batifol, Andreas Blattmann, Frederic Boesel, Saksham Consul, Cyril Diagne, Tim Dockhorn, Jack English, Zion English, Patrick Esser, Sumith Kulal, Kyle Lacey, Yam Levi, Cheng Li, Dominik Lorenz, Jonas Müller, Dustin Podell, Robin Rombach, Harry Saini, Axel Sauer, and Luke Smith. 2025. FLUX.1 Kontext: Flow Matching for In-Context Image Generation and Editing in Latent Space. *arXiv:2506.15742 [cs.GR]* <https://arxiv.org/abs/2506.15742>
- Zeqiang Lai, Yunfei Zhao, Haolin Liu, Zibo Zhao, Qingxiang Lin, Huiwen Shi, Xianghui Yang, Mingxin Yang, Shuhui Yang, Yifei Feng, et al. 2025. Hunyuan3D 2.5: Towards High-Fidelity 3D Assets Generation with Ultimate Details. *arXiv preprint arXiv:2506.16504* (2025).
- Biwen Lei, Jianqiang Ren, Mengyang Feng, Miaomiao Cui, and Xuansong Xie. 2023. A hierarchical representation network for accurate and detailed face reconstruction from in-the-wild images. In *Proceedings of the IEEE/CVF Conference on Computer Vision and Pattern Recognition*. 394–403.
- Bruno Lévy, Sylvain Petitjean, Nicolas Ray, and Jérôme Maillot. 2023. Least squares conformal maps for automatic texture atlas generation. In *Seminal Graphics Papers: Pushing the Boundaries, Volume 2*. 193–202.
- Tianye Li, Timo Bolkart, Michael J Black, Hao Li, and Javier Romero. 2017. Learning a model of facial shape and expression from 4D scans. *ACM Trans. Graph.* 36, 6 (2017), 194–1.
- Tianye Li, Shichen Liu, Timo Bolkart, Jiayi Liu, Hao Li, and Yajie Zhao. 2021. Topologically consistent multi-view face inference using volumetric sampling. In *Proceedings of the IEEE/CVF International Conference on Computer Vision*. 3824–3834.
- Yanjie Li, Sen Yang, Peidong Liu, Shoukui Zhang, Yunxiao Wang, Zhicheng Wang, Wankou Yang, and Shu-Tao Xia. 2022. Simcc: A simple coordinate classification perspective for human pose estimation. In *European Conference on Computer Vision*. Springer, 89–106.
- Zhihao Li, Yufei Wang, Heliang Zheng, Yihao Luo, and Bihan Wen. 2025. Sparc3D: Sparse Representation and Construction for High-Resolution 3D Shapes Modeling.

- arXiv preprint arXiv:2505.14521* (2025).
- Ruofan Liang, Zan Gojic, Huan Ling, Jacob Munkberg, Jon Hasselgren, Chih-Hao Lin, Jun Gao, Alexander Keller, Nandita Vijaykumar, Sanja Fidler, et al. 2025. Diffusion Renderer: Neural Inverse and Forward Rendering with Video Diffusion Models. In *Proceedings of the Computer Vision and Pattern Recognition Conference*. 26069–26080.
- Yaron Lipman, Ricky TQ Chen, Heli Ben-Hamu, Maximilian Nickel, and Matt Le. 2022. Flow matching for generative modeling. *arXiv preprint arXiv:2210.02747* (2022).
- Ziwei Liu, Ping Luo, Xiaoogang Wang, and Xiaoou Tang. 2015. Deep Learning Face Attributes in the Wild. In *Proceedings of International Conference on Computer Vision (ICCV)*.
- Marcel Lüthi, Thomas Gerig, Christoph Jud, and Thomas Vetter. 2017. Gaussian process morphable models. *IEEE transactions on pattern analysis and machine intelligence* 40, 8 (2017), 1860–1873.
- Chengqi Lyu, Wenwei Zhang, Haian Huang, Yue Zhou, Yudong Wang, Yanyi Liu, Shilong Zhang, and Kai Chen. 2022. Rtmtdet: An empirical study of designing real-time object detectors. *arXiv preprint arXiv:2212.07784* (2022).
- Wan-Chun Ma, Tim Hawkins, Pieter Peers, Charles-Felix Chabert, Malte Weiss, Paul E Debevec, et al. 2007. Rapid Acquisition of Specular and Diffuse Normal Maps from Polarized Spherical Gradient Illumination. *Rendering Techniques* 9, 10 (2007), 2.
- Mark Meyer, Mathieu Desbrun, Peter Schröder, and Alan H Barr. 2003. Discrete differential-geometry operators for triangulated 2-manifolds. In *Visualization and mathematics III*. Springer, 35–57.
- Ben Mildenhall, Pratul P Srinivasan, Matthew Tancik, Jonathan T Barron, Ravi Ramamoorthi, and Ren Ng. 2021. Nerf: Representing scenes as neural radiance fields for view synthesis. *Commun. ACM* 65, 1 (2021), 99–106.
- Andriy Myronenko and Xubo Song. 2010. Point set registration: Coherent point drift. *IEEE transactions on pattern analysis and machine intelligence* 32, 12 (2010), 2262–2275.
- Adam Paszke, Sam Gross, Francisco Massa, Adam Lerer, James Bradbury, Gregory Chanan, Trevor Killeen, Zeming Lin, Natalia Gimelshein, Luca Antiga, Alban Desmaison, Andreas Kopf, Edward Yang, Zachary DeVito, Martin Raison, Alykhan Tejani, Sasank Chilamkurthy, Benoit Steiner, Lu Fang, Junjie Bai, and Soumith Chintala. 2019. PyTorch: An Imperative Style, High-Performance Deep Learning Library. In *Advances in Neural Information Processing Systems*. 8024–8035.
- Pascal Paysan, Reinhard Knothe, Brian Amberg, Sami Romdhani, and Thomas Vetter. 2009. A 3D face model for pose and illumination invariant face recognition. In *2009 sixth IEEE international conference on advanced video and signal based surveillance*. Ieee, 296–301.
- Nick Pears, Hang Dai, Will Smith, and Hao Sun. 2023. Laplacian ICP for progressive registration of 3D human head meshes. In *2023 IEEE 17th International Conference on Automatic Face and Gesture Recognition (FG)*. IEEE, 1–7.
- William Peebles and Saining Xie. 2023. Scalable diffusion models with transformers. In *Proceedings of the IEEE/CVF international conference on computer vision*. 4195–4205.
- Stylianios Ploumpis, Haoyang Wang, Nick Pears, William AP Smith, and Stefanos Zafeiriou. 2019. Combining 3d morphable models: A large scale face-and-head model. In *Proceedings of the IEEE/CVF conference on computer vision and pattern recognition*. 10934–10943.
- Lingteng Qiu, Xiaodong Gu, Peihao Li, Qi Zuo, Weichao Shen, Junfei Zhang, Kejie Qiu, Weihao Yuan, Guanying Chen, Zilong Dong, et al. 2025. Lhm: Large animatable human reconstruction model from a single image in seconds. *arXiv preprint arXiv:2503.10625* (2025).
- Anurag Ranjan, Timo Bolkart, Soubhik Sanyal, and Michael J Black. 2018. Generating 3D faces using convolutional mesh autoencoders. In *Proceedings of the European conference on computer vision (ECCV)*. 704–720.
- Christian Ratz. 2017. NormalmapGenerator: A simple program that converts images into normal maps. <https://github.com/Theverat/NormalmapGenerator>.
- Nikhila Ravi, Jeremy Reizenstein, David Novotny, Taylor Gordon, Wan-Yen Lo, Justin Johnson, and Georgia Gkioxari. 2020. Accelerating 3D Deep Learning with PyTorch3D. In *SIGGRAPH Asia 2020 Courses*. 1–1.
- George Retsinas, Panagiotis P Filntsis, Radek Danecsek, Victoria F Abrevaya, Anastasios Roussos, Timo Bolkart, and Petros Maragos. 2024. SMIRK: 3D Facial Expressions through Analysis-by-Neural-Synthesis. *arXiv preprint arXiv:2404.04104* (2024).
- Elad Richardson, Matan Sela, Roy Or-El, and Ron Kimmel. 2017. Learning detailed face reconstruction from a single image. In *Proceedings of the IEEE conference on computer vision and pattern recognition*. 1259–1268.
- Matan Sela, Elad Richardson, and Ron Kimmel. 2017. Unrestricted facial geometry reconstruction using image-to-image translation. In *Proceedings of the IEEE international conference on computer vision*. 1576–1585.
- Olga Sorkine and Marc Alexa. 2007. As-rigid-as-possible surface modeling. In *Symposium on Geometry processing*, Vol. 4. 109–116.
- Farzam Tajdari, Toon Huysmans, Yusheng Yang, and Yu Song. 2022. Feature preserving non-rigid iterative weighted closest point and semi-curvature registration. *IEEE Transactions on Image Processing* 31 (2022), 1841–1856.
- Felix Taubner, Prashant Raina, Mathieu Tuli, Eu Wern Teh, Chul Lee, and Jimmiao Huang. 2024. 3D face tracking from 2D video through iterative dense UV to image flow. In *Proceedings of the IEEE/CVF Conference on Computer Vision and Pattern Recognition*. 1227–1237.
- Luan Tran and Xiaoming Liu. 2018. Nonlinear 3d face morphable model. In *Proceedings of the IEEE conference on computer vision and pattern recognition*. 7346–7355.
- Ashish Vaswani, Noam Shazeer, Niki Parmar, Jakob Uszkoreit, Llion Jones, Aidan N Gomez, Lukasz Kaiser, and Illia Polosukhin. 2017. Attention is all you need. *Advances in neural information processing systems* 30 (2017).
- Noranart Vesdapunt, Mitch Rundle, HsiangTao Wu, and Baoyuan Wang. 2020. JNR: Joint-based neural rig representation for compact 3D face modeling. In *European Conference on Computer Vision*. Springer, 389–405.
- Daniel Vlasic, Matthew Brand, Hanspeter Pfister, and Jovan Popovic. 2006. Face transfer with multilinear models. In *ACM SIGGRAPH 2006 Courses*. 24–es.
- Jianyuan Wang, Minghao Chen, Nikita Karaev, Andrea Vedaldi, Christian Rupprecht, and David Novotny. 2025. Vggg: Visual geometry grounded transformer. In *Proceedings of the Computer Vision and Pattern Recognition Conference*. 5294–5306.
- Lizhen Wang, Zhiyuan Chen, Tao Yu, Chenguang Ma, Liang Li, and Yebin Liu. 2022. Faceverse: a fine-grained and detail-controllable 3d face morphable model from a hybrid dataset. In *Proceedings of the IEEE/CVF conference on computer vision and pattern recognition*. 20333–20342.
- Peng Wang, Lingjie Liu, Yuan Liu, Christian Theobalt, Taku Komura, and Wenping Wang. 2021. Neus: Learning neural implicit surfaces by volume rendering for multi-view reconstruction. *arXiv preprint arXiv:2106.10689* (2021).
- Tengfei Wang, Bo Zhang, Ting Zhang, Shuyang Gu, Jianmin Bao, Tadas Baltrusaitis, Jingjing Shen, Dong Chen, Fang Wen, Qifeng Chen, et al. 2023. Rodin: A generative model for sculpting 3d digital avatars using diffusion. In *Proceedings of the IEEE/CVF conference on computer vision and pattern recognition*. 4563–4573.
- Xintao Wang, Liangbin Xie, Chao Dong, and Ying Shan. 2021. Real-ESRGAN: Training Real-World Blind Super-Resolution with Pure Synthetic Data. In *International Conference on Computer Vision Workshops (ICCVW)* (2021).
- Yue Wu, Yufan Wu, Wen Li, Yuxi Lu, Kairui Feng, and Xuanhong Chen. 2025. FastAvatar: Towards Unified Fast High-Fidelity 3D Avatar Reconstruction with Large Gaussian Reconstruction Transformers. *arXiv preprint arXiv:2508.19754* (2025).
- Jianfeng Xiang, Zelong Lv, Sicheng Xu, Yu Deng, Ruicheng Wang, Bowen Zhang, Dong Chen, Xin Tong, and Jiaolong Yang. 2025. Structured 3d latents for scalable and versatile 3d generation. In *Proceedings of the Computer Vision and Pattern Recognition Conference*. 21469–21480.
- Hongyi Xu, Eduard Gabriel Bazavan, Andrei Zanfir, William T Freeman, Rahul Sukthankar, and Cristian Sminchisescu. 2020. Ghum & ghuml: Generative 3d human shape and articulated pose models. In *Proceedings of the IEEE/CVF Conference on Computer Vision and Pattern Recognition*. 6184–6193.
- Valikhujaev Yakhokhuja. 2024. face-parsing. <https://github.com/yakhyo/face-parsing>. GitHub repository.
- Haotian Yang, Hao Zhu, Yanru Wang, Mingkai Huang, Qiu Shen, Ruigang Yang, and Xun Cao. 2020. Facescape: a large-scale high quality 3d face dataset and detailed riggable 3d face prediction. In *Proceedings of the IEEE/CVF conference on computer vision and pattern recognition*. 601–610.
- Kai Yang, Hong Shang, Tianyang Shi, Xinghan Chen, Jingkai Zhou, Zhongqian Sun, and Wei Yang. 2023. Asm: Adaptive skinning model for high-quality 3d face modeling. In *Proceedings of the IEEE/CVF International Conference on Computer Vision*. 20708–20717.
- Yusuke Yoshiyasu, Wan-Chun Ma, Eiichi Yoshida, and Fumio Kanehiro. 2014. As-conformal-as-possible surface registration. In *Computer Graphics Forum*, Vol. 33. Wiley Online Library, 257–267.
- Xiaoxing Zeng, Xiaojiang Peng, and Yu Qiao. 2019. Df2net: A dense-fine-finer network for detailed 3d face reconstruction. In *Proceedings of the IEEE/CVF International Conference on Computer Vision*. 2315–2324.
- Biao Zhang, Jiapeng Tang, Matthias Niessner, and Peter Wonka. 2023b. 3dshape2vecset: A 3d shape representation for neural fields and generative diffusion models. *ACM Transactions On Graphics (TOG)* 42, 4 (2023), 1–16.
- Longwen Zhang, Qiwei Qiu, Hongyang Lin, Qixuan Zhang, Cheng Shi, Wei Yang, Ye Shi, Sibe Yang, Lan Xu, and Jingyi Yu. 2023a. DreamFace: Progressive Generation of Animatable 3D Faces under Text Guidance. arXiv:2304.03117 [cs.GR] <https://arxiv.org/abs/2304.03117>
- Longwen Zhang, Ziyu Wang, Qixuan Zhang, Qiwei Qiu, Anqi Pang, Haoran Jiang, Wei Yang, Lan Xu, and Jingyi Yu. 2024. Clay: A controllable large-scale generative model for creating high-quality 3d assets. *ACM Transactions on Graphics (TOG)* 43, 4 (2024), 1–20.
- Mingwu Zheng, Hongyu Yang, Di Huang, and Liming Chen. 2022. Imface: A nonlinear 3d morphable face model with implicit neural representations. In *Proceedings of the IEEE/CVF conference on computer vision and pattern recognition*. 20343–20352.
- Wojciech Zielonka, Timo Bolkart, and Justus Thies. 2022. Towards metrical reconstruction of human faces. In *European conference on computer vision*. Springer, 250–269.

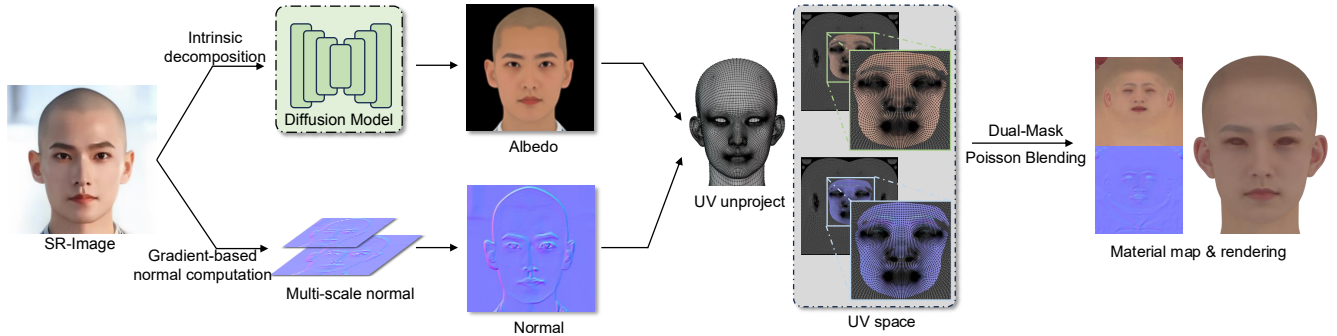


Fig. 4. **Pipeline of texture extraction.** The input image is first super-resolved and decomposed to obtain albedo, while a heuristic normal map is estimated in image space. Both albedo and normal maps are then projected onto the UV map via rasterization, preserving high-frequency details. Finally, missing regions due to self-occlusion are completed using Dual-Mask Poisson Blending to ensure color and gradient consistency.

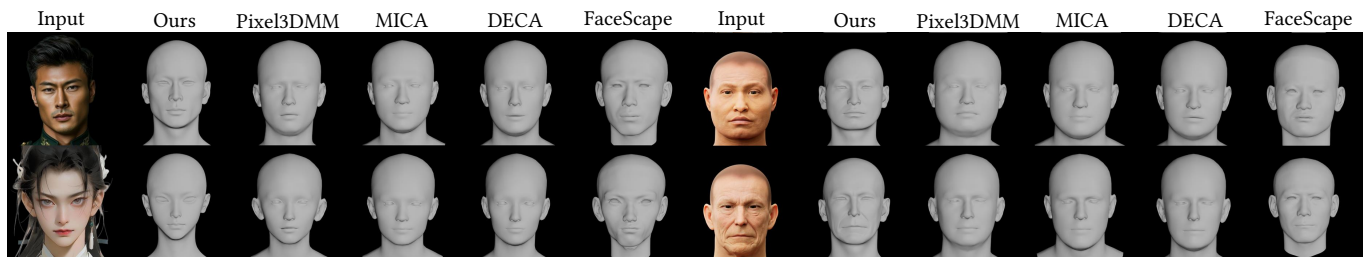


Fig. 5. **Comparison of single-image head reconstruction methods on *in-the-wild* and *synthetic* datasets.** The two rows on the left show results on *in-the-wild* images, while the two rows on the right present reconstructions on synthetic data. Across both settings, our method produces noticeably more realistic and identity-faithful heads than existing methods.

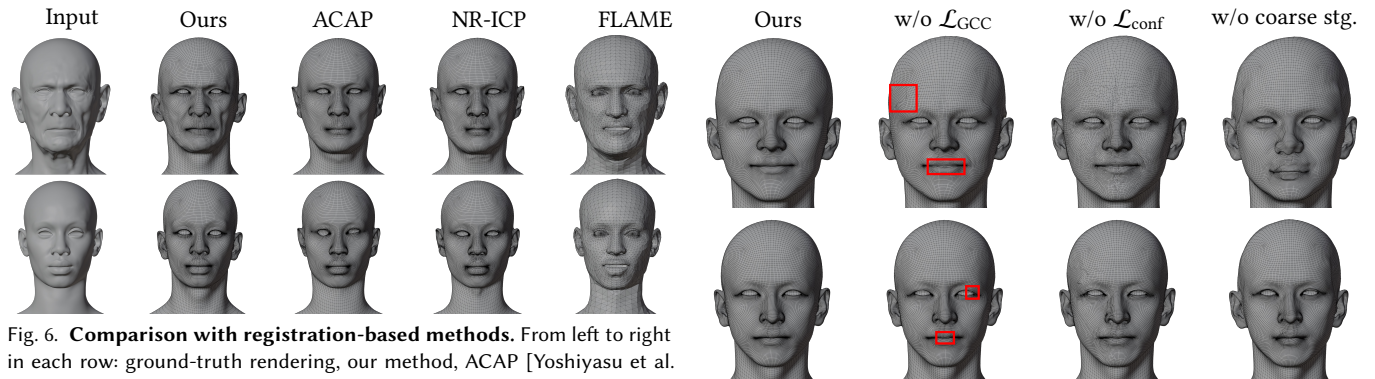


Fig. 6. **Comparison with registration-based methods.** From left to right in each row: ground-truth rendering, our method, ACAP [Yoshiyasu et al. 2014], NR-ICP [Amberg et al. 2007], and FLAME [Li et al. 2017]. Benefiting from our coarse-to-fine framework and geometry-aware regularization, our method reconstructs head geometry with topology regularity comparable to registration-based approaches.

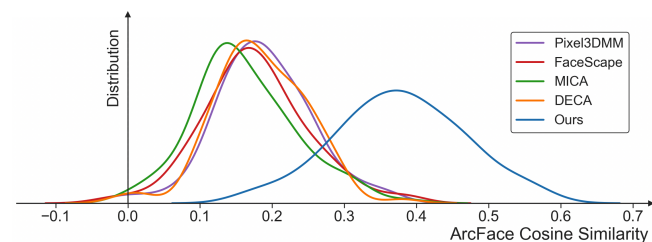


Fig. 7. **ArcFace score distribution on the synthetic dataset.** Our method (blue) yields consistently higher ArcFace scores than other single-image approaches on this evaluation set.

Fig. 8. **Ablation study of our regularizations and coarse-to-fine framework.** From left to right: our method, results without Edge-to-Vertex Gaussian Curvature Constraint, results without angle preservation constraints, and direct vertex-level optimization. The local artifacts caused by removing EV-GCC are highlighted with red boxes for clarity, making it easier to identify the artifacts introduced by this modification.

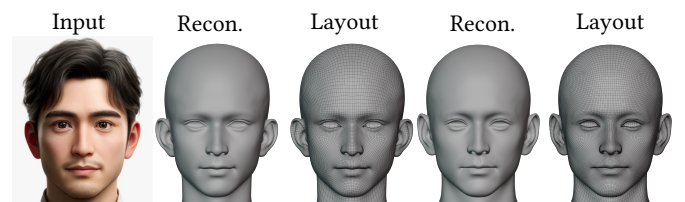


Fig. 9. **Qualitative evaluation on different head-mesh topologies.** From left to right: input image, reconstruction with a simplified topology, its mesh layout, reconstruction with MetaHuman topology, and its mesh layout. Our method preserves identity and produces clean, semantically consistent topology in both settings.



Fig. 10. Comparison with DreamFace. Each row from left to right: input image, our reconstruction, and DreamFace reconstruction, repeated for two examples. Our method better preserves global facial structure and fine-grained details in these examples.



Fig. 11. More reconstruction and downstream deformation results produced by our method. From left to right: the input image, reconstructed geometry, mesh topology, textured reconstruction, and a sequence of extreme deformation tests. These examples show that our reconstructed meshes remain stable in challenging downstream deformation tests.